Icarus xxx (2009) xxx–xxx

Contents lists available at ScienceDirect

Icarus

journal homepage: www.elsevier.com/locate/icarus

The sodium tail of the Moon

M. Matta [a,b,*], S. Smith [a,1], J. Baumgardner [a,1], J. Wilson [a,1], C. Martinis [a,1], M. Mendillo [b,1]

[a] Center for Space Physics, Boston University, 725 Commonwealth Ave., Boston, MA 02215, USA
[b] Department of Astronomy, Boston University, 725 Commonwealth Ave., Boston, MA 02215, USA

ARTICLE INFO

Article history:
Received 6 March 2009
Revised 1 June 2009
Accepted 22 June 2009
Available online xxxx

Keywords:
Moon
Meteors
Solar wind
Solar radiation
Image processing

ABSTRACT

During the few days centered about new Moon, the lunar surface is optically hidden from Earth-based observers. However, the Moon still offers an observable: an extended sodium tail. The lunar sodium tail is the escaping "hot" component of a coma-like exosphere of sodium generated by photon-stimulated desorption, solar wind sputtering and meteoroid impact. Neutral sodium atoms escaping lunar gravity experience solar radiation pressure that drives them into the anti-solar direction forming a comet-like tail. During new Moon time, the geometry of the Sun, Moon and Earth is such that the anti-sunward sodium flux is perturbed by the terrestrial gravitational field resulting in its focusing into a dense core that extends beyond the Earth. An all-sky camera situated at the El Leoncito Observatory (CASLEO) in Argentina has been successfully imaging this tail through a sodium filter at each lunation since April 2006. This paper reports on the results of the brightness of the lunar sodium tail spanning 31 lunations between April 2006 and September 2008. Brightness variability trends are compared with both sporadic and shower meteor activity, solar wind proton energy flux and solar near ultra violet (NUV) patterns for possible correlations. Results suggest minimal variability in the brightness of the observed lunar sodium tail, generally uncorrelated with any single source, yet consistent with a multi-year period of minimal solar activity and non-intense meteoric fluxes.

1. Introduction

The lunar atmosphere is a tenuous exosphere resulting from the continuous release and subsequent loss of neutral species from its surface. It is often referred to as a surface-boundary-exosphere (SBE), or a "transient" atmosphere (Hunten and Sprague, 1997; Stern, 1999). Following a post-Apollo dormancy in lunar studies, the discovery of sodium and potassium emission spectra in the lunar environment (Potter and Morgan, 1988a,b; Tyler et al., 1988) from ground-based facilities sparked new interest in the Moon. Subsequent two-dimensional images of the Moon's extended exosphere at various lunar phases (Mendillo et al., 1991, 1993; Flynn and Mendillo, 1993; Potter and Morgan, 1998) showed a bound sodium atmosphere that spans $\sim 5\ R_M$ ($R_M = 1$, lunar radius = 1738 km) on the day-side at the sub-solar point and an escaping component up to $\sim 20\ R_M$ on the night side. That is, the Moon has an extended sodium tail.

A novel observing technique for lunar science was discovered soon after the 1998 Leonid meteor shower (Smith et al., 1999). On 19 November 1998, an all-sky camera at the McDonald Observatory in Texas used to observe waves in the terrestrial sodium layer revealed an unusual $\sim 3^\circ \times 3^\circ$ bright feature in the anti-sun direction. Subsequent modeling studies (Wilson et al., 1999) showed it to be the tail of neutral sodium atoms escaping the Moon that, for the Sun–Moon–Earth aligned geometry of the new Moon phase, had been focused by the Earth's gravitational field into a narrow column of emission. Fig. 1 illustrates this situation. The Wilson et al. (1999) study showed that at new Moon the lunar sodium tail extended out to about 400,000 km ($\sim 230\ R_M$), and that it took approximately 2 days for sodium atoms leaving the Moon to reach the Earth's vicinity. Thus, the observed "Na spot" detected on 19 November 1998 was traced back to the Leonid meteor shower peak on 17 November 1998.

Sodium escapes the lunar surface throughout the lunar cycle. As illustrated in Fig. 1, the sampling geometry is different for each phase of the optically visible Moon. Earth-based brightness measurements therefore integrate along a line of sight that traverses a lunar sodium feature (e.g., the day-side coma) at a certain angle. The ray path is nearly perpendicular to the sodium tail at the quarter Moon phases. These methods sample a population of sodium that left the lunar surface some hours ago, and they overlap only a small portion of the ray path. When the Moon is near its new phase, Earth-based brightness measurements of the extended lunar sodium tail, however, integrate along a line of sight that is co-aligned with the axis of the tail, extending out to beyond $\sim 120\ R_E$ ($\sim 440\ R_M$) from the Moon. This method samples a popu-

* Corresponding author. Fax: +1 617 353 6563.
E-mail addresses: majdm@bu.edu (M. Matta), smsm@bu.edu (S. Smith), jeffreyb@bu.edu (J. Baumgardner), jkwilson@bu.edu (J. Wilson), martinis@bu.edu (C. Martinis), mendillo@bu.edu (M. Mendillo).
[1] Fax: +1 617 353 6563.

0019-1035/$ - see front matter © 2009 Elsevier Inc. All rights reserved.
doi:10.1016/j.icarus.2009.06.017

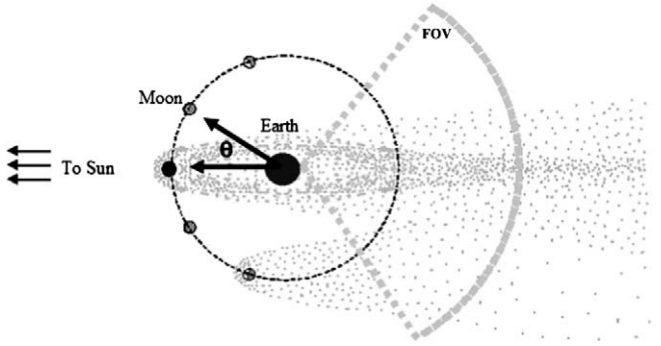

Fig. 1. Projection onto the ecliptic of the Sun–Moon–Earth configuration during the few days about new Moon. The dotted region represents the effective field of view used of the all-sky camera (~120°). This new Moon time geometry allows for lunar sodium tail formation and detection (see text). The depiction of the lunar tail at a phase near first quarter is shown to illustrate a geometry where terrestrial gravity does not focus the tail into a spot (figure not drawn to scale). The angle θ is the Sun–Earth–Moon angle.

lation of sodium that left the Moon over a span of several days. Such brightness measurements of the extended lunar sodium tail around new Moon are fundamentally different than those made of the lunar tail throughout remaining lunar phases. Hence, no single method allows for continuous measuring of the lunar sodium tail throughout the lunar cycle.

In this paper, we concentrate on measurements of the lunar sodium tail spot, the observational appearance of the tail, as seen from the night side of Earth on nights near new Moon. Two-dimensional brightness measurements of the spot show it to have different shapes: circles to ovals to arches tilted to the east or west, depending on time observed away from strict new Moon (Smith et al., 1999; Wilson et al., 1999; Shiokawa et al., 2000).

The major sources and sinks of neutral species in the lunar environment are well summarized in Stern's (1999) review. The source processes relevant to sodium are: thermal desorption, photon-stimulated desorption, meteoric impact and charged particle sputtering. The relevant loss processes are similar to those experienced by comets: gravitational escape, photo-ionization with subsequent plasma pick-up by the solar wind, and the dispersal of neutral gases by solar radiation pressure, with the latter two processes dominating lunar loss processes. Re-supply to the lunar regolith (the loose surface layer) comes from meteorites, solar wind and previously escaped neutrals that are turned back to the surface by solar radiation pressure. There is some debate as to which source is the one responsible for producing fast neutral sodium on the lunar surface, i.e., the population that leads to the extended tail (Bruno et al., 2007). We address these issues using a new 2.5 year data set of the lunar sodium spot.

2. Observations

The Boston University all-sky imager at the El Leoncito Observatory in Argentina (31.8°S, 69.3°W) consists of a 16 mm focal length (FL) fisheye lens coupled optically to an Andor DW436 CCD camera. The 40 mm output image formed by the fisheye lens is collimated by a 340 mm FL f/3 objective and filtered by one of six narrow-band interference filters arranged in a filter wheel. The two filters of interest to this work are the sodium filter (centered at 5893 Å, with a FWHM of 14.3 Å and peak transmission of 56%) and a control filter (centered at 6444 Å with a FWHM of 14.6 Å and a peak transmission of 75%). These and the four remaining filters are used for observations of emissions from the Earth's mesosphere and thermosphere. The sodium filter bandwidth allows simultaneous observation of both D_1 and D_2 lines at 5896 Å and 5890 Å, respectively. After passing through the filter plane, the image is re-formed by a 135 mm FL f/1.5 lens into the CCD. Fig. 2 shows a schematic of the all-sky camera used at El Leoncito. Table 1 lists details of the detector used. Sodium and control images are obtained via 120 s integrations and are separated temporally by 267 s. The control image is used to remove the background continuum. The cycle time for any given filter is ~12 min. For a more complete description of all-sky imaging systems, see Baumgardner et al. (1993).

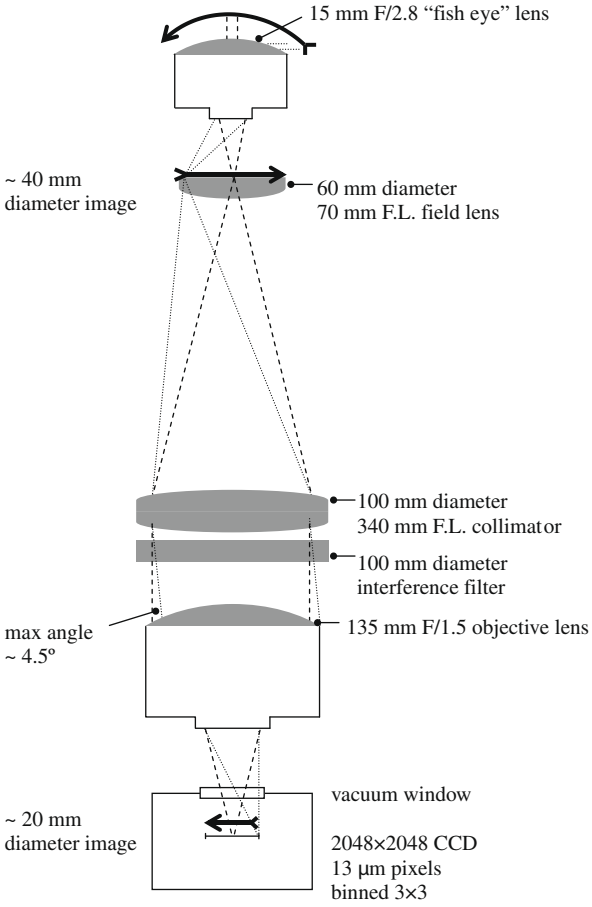

Fig. 2. Schematic of the all-sky camera used for the observations at El Leoncito, Argentina.

Here we report on observations that span 30 continuous months during which 31 new Moons occurred. While all-sky observations were made nightly, those made during the five nights centered about new Moon resulted in 155 nights being systematically analyzed for sodium tail signatures. We have been successful in detecting the extended lunar sodium tail for at least one night (and up to three nights) during each lunation. Photometric calibrations into brightness values in Rayleighs (R) were obtained for 58 nights over 2.5 years of new Moon periods. All observations were made from the same location using the same observing system and comprise the largest data set to date for sodium of lunar origin taken continuously at monthly intervals (see Table 2).

Typically, observations begin approximately 1 h after sunset and end 1 h before sunrise. Depending on season at El Leoncito, start time is between ~22 and ~00 UT (Universal Time = Local Time – 4 h), and end time is between ~08 and ~11 UT. Between 40 and 60 sodium and control image pairs were obtained for each night of interest in the lunation periods between April 2006 and October 2008. The lunar sodium tail signature spot is typically most visible in a subset of these sodium images nearest local mid-

Please cite this article in press as: Matta, M., et al. The sodium tail of the Moon. Icarus (2009), doi:10.1016/j.icarus.2009.06.017

Table 1
Summary of all-sky camera detector parameters.

Detector size	2048 × 2048 array with 13.5 μm square pixels. The images are 3 × 3 binned before readout resulting in a 682 × 682 pixel array
Dark current	<0.2 e^- $pixel^{-1}$ s^{-1} at −55 °C
Plate scale	~0.35° $pixel^{-1}$
Quantum efficiency	~90% for our wavelength range (for sodium D_1, D_2 and 6444 Å)
Read noise (r.m.s.)	4 e^- @ 2 μs $cycle^{-1}$
Field of view	180° circular (we use the innermost ~120° to avoid vignetting and atmospheric extinction effects at the edge of the field of view)
FWHM of typical star	~3 pixels

night. Sample sodium all-sky images are shown in Fig. 3 as raw data in panels (a) and (b) and as reduced images (dark and background subtracted then smoothed) in panels (c) and (d).

Although the lunar sodium tail is visible for every lunation in all months of observations, intermittent clouds affect the ability to obtain rigorously calibrated images for each night observed. Between April 2006 and October 2008, a total of 7079 images were analyzed, of which 1239 had visible lunar sodium tails of photometric quality. Table 3 summarizes the distribution of nights with observable photometric lunar sodium during five-day periods spanning new Moon.

3. Image processing

Processing all-sky images to determine brightness values for the observed lunar sodium tails is a three-step process. First, the images must be reduced to account for extinction, vignetting and broadband and terrestrial atmospheric sodium effects. Next, the spot brightness is calibrated using standard stars to obtain a brightness value in Rayleighs. Finally, a correction is made for the position of the Moon with respect to the Earth and Sun to standardize brightness values to similar geometrical conditions.

Table 2
Summary of published observations of lunar sodium.

Reference	Observational media	Nights observed
This work	All-sky images of distant tail	58
Wilson et al. (2006)	Coronagraphic image	5*
Mierkiewicz et al. (2006)	Spectra	3
Verani et al. (2001)	Spectra	2
Barbieri et al. (2001)	Spectra	6
Smith et al. (2001)	All-sky images of distant tail	8
Shiokawa et al. (2000)	All-sky images of distant tail	5
Potter et al. (2000)	Spectra	10
Smith et al. (1999)	All-sky images of distant tail	5
Mendillo et al. (1999)	Coronagraphic image	3
Verani et al. (1998)	Spectra	2
Potter and Morgan (1998)	Coronagraphic image	1
Hunten et al. (1998)	Spectra	3
Sprague et al. (1998)	Spectra	4
Cremonese and Verani (1997)	Spectra	6
Contarini et al. (1996)	Spectra	2
Mendillo and Baumgardner (1995)	Coronagraphic image	1
Stern and Flynn (1995)	Narrow-field spectral imaging	2
Potter and Morgan (1994)	Spectra	<19*
Mendillo et al. (1993)	Coronagraphic image	2
Sprague et al. (1992)	Spectra	12
Potter and Morgan (1991)	Spectra	6
Mendillo et al. (1991)	Coronagraphic image	1
Hunten et al. (1991)	Spectra	4
Tyler et al. (1988)	Spectra	2
Potter and Morgan (1988b)	Spectra	2
Potter and Morgan (1988a)	Spectra	4

* Indicate a total of old and new observations.

3.1. Image reduction

For each night studied, all of the 120 s dark exposures (typically taken at the beginning and end of each observing session) are averaged to generate one dark image to be used for that night. The resulting average dark image is subtracted from both the sodium and control images. All images are then normalized to 1 s exposure time. The control images are rotated about the south celestial pole to account for the 267 s offset in the time the control image was captured to the time the corresponding sodium image was captured. We find that an empirically-determined factor of 0.63 of the control image needs to be subtracted from the sodium image to eliminate the Milky Way (the broadest band source of background light in the image). This factor is due to the area under the filters used, the quantum efficiency of the CCD at the wavelengths used, and the optical system efficiency. The brightness of the lunar sodium tail is calibrated to one of the many standard stars available. An average value of 9 pixels (from a 3 × 3 pixel box) centered about the brightest pixel in the imaged spot is used to derive brightness values. Four boxes of similar size to the lunar sodium sample are chosen away from the spot at comparable zenith distance and averaged to determine background terrestrial sodium emissions. The background value is then subtracted from the lunar spot image. Finally, images are divided by the transmission of the sodium filter to create images for an equivalent 100% transmission. This calibration process dynamically corrects for vignetting, atmospheric extinction, background sodium emissions, terrestrial sodium emissions and filter transmission on a nightly basis. Thus, all subsequent brightness values in R are quoted as "above the terrestrial atmosphere" values.

3.2. Brightness calibration

The brightness of the lunar tail within the sodium image is calibrated using mostly B, A, F and G-type standard stars. Standard star candidates are those that remain visible for the duration of the observing night. A number of stars with a distribution of air-mass per image are used each night for calibration based on their seasonal visibility above the horizon. Motion of the standard stars from all images in a given night are used to map out the change in star brightness with air-mass, a function referred to as 'sensitivity', and one that accounts for both extinction and vignetting. Sensitivity values represent the Rayleigh-second per data number (R s DN^{-1}) of each pixel. The resulting reduced sodium images (in DN s^{-1}) are multiplied by this sensitivity to generate an image with pixel values in Rayleighs (R).

A tutorial by Wilson (http://sirius.bu.edu/planetary/obstools/starflux/starcalib/starcalib.htm) demonstrates how to calibrate an all-sky image into Rayleighs using standard stars. Briefly:

$$B = 10^{-6} \times 4\pi F_A/\omega \text{ (in R)}$$

where B is the brightness in Rayleighs, F_A is the airless flux above the atmosphere of a standard star (in photons cm^{-2} s^{-1}) detected by the all-sky camera ($F_A = F \times SW$, where F is the flux of a star in photons cm^{-2} s^{-1} $Å^{-1}$ and SW is the spectral width ~ FWHM × Transmission). The solid angle ω extended by the pixels of the lunar sodium tail is a function of pixel location and can be determined by:

$$\omega(r) = 180^\circ \sin(z(r)) \times z'(r)/(\pi r)$$

where $z(r)$ and $z'(r)$ are the system-specific distortion function and its derivative that map pixel radius r from the center of an all-sky image (taken to be at zenith) to zenith angle.

Given the flux F of a star, an image in DN, a filter with known spectral width in Å, and a location in an all-sky camera image (x and y coordinates in pixels), we generate a sensitivity map that assigns each pixel in an all-sky image to a sensitivity value (in

Please cite this article in press as: Matta, M., et al. The sodium tail of the Moon. Icarus (2009), doi:10.1016/j.icarus.2009.06.017

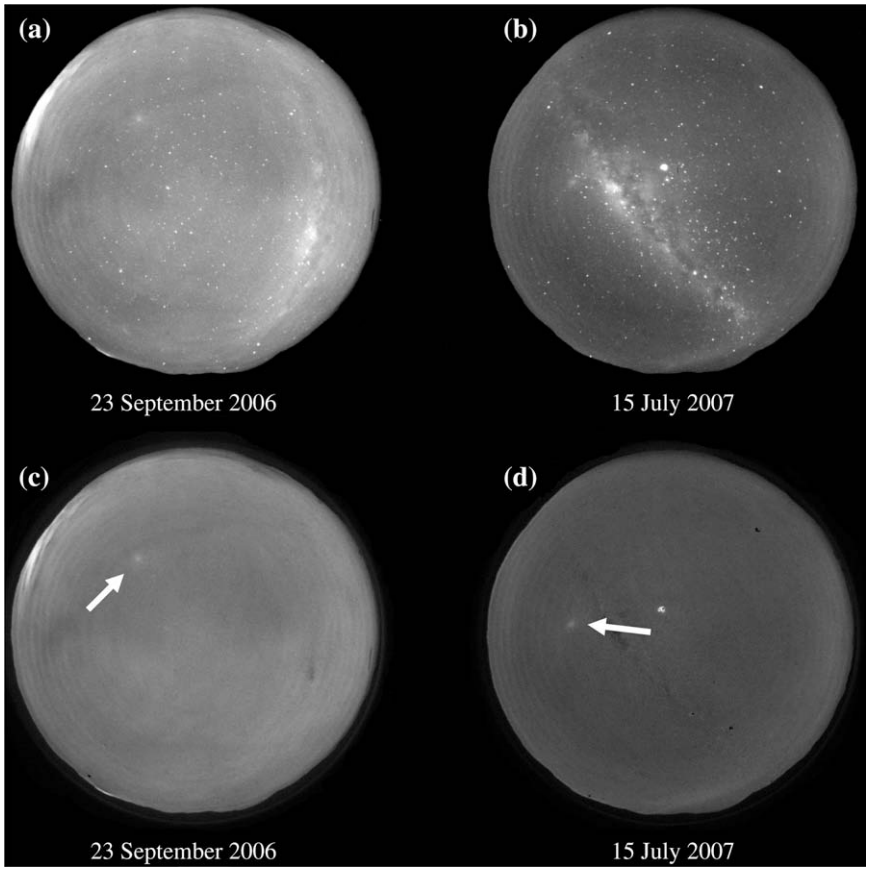

Fig. 3. Sample of all-sky images showing lunar sodium spots. Panels (a) and (b) are raw images taken by the El Leoncito Observatory all-sky camera for 23 September 2006 and 15 July 2007, respectively. Panels (c) and (d) are the same images after they have been dark-subtracted, off-band subtracted, and smoothed. The Milky Way is clearly visible in (a) and (b). The bright feature near zenith (center) in panels (b) and (d) is Jupiter.

Table 3
Distribution of observations spanning new Moon conditions.

Night	Number of nights with photometric lunar tail brightness calibrations
New Moon – 2 nights	0
New Moon – 1 night	2
New Moon night	17
New Moon + 1 night	27
New Moon + 2 nights	12

R s DN^{-1}) from which the brightness of a pixel in Rayleighs can be calculated.

3.3. Correcting for geometry effects

The 1239 images used to calibrate the lunar sodium tail into Rayleighs span four nights around new Moon conditions, and therefore each represents a brightness of the lunar tail for a particular geometry of the Moon with respect to the Earth and Sun, as noted in Table 2. To eliminate brightness variability due to this effect, a correction is required to determine brightness values representative of the same geometry. A plot of the calibrated lunar sodium tail brightness values in Rayleighs vs. Sun–Earth–Moon angle (angle θ introduced in Fig. 1) is shown in Fig. 4. This figure shows the lunar sodium tail brightness decreasing with increasing aspect angle and is best-fit by an exponential decay function. The fit is made using two-degree binned averages of the brightness values and shows an agreement with the total trend in brightness. Dividing individual brightness values by this fit is used to normalize all measurements to strict new Moon phase geometry (that closest to solar eclipse alignment) to allow for position-independent comparisons. Resulting brightness values represent a similar geometric configuration where the Sun, Moon and Earth are near-aligned and show a sample average of 78 R.

Using the results in Fig. 4, we geometrically corrected the observed Moon spot brightness values for each night and present their night-by-night average values in Fig. 5. Since only a few other studies have made lunar tail measurements using all-sky cameras, limited cases exist where it is possible to compare our results with others. Using our calibration method described above, we found sodium images from the McDonald Observatory during the post-1998 Leonid period, where the distant lunar sodium tail was discovered (Smith et al., 1999), to give good agreement. Mierkiewicz et al. (2006) made brightness measurements of the lunar sodium D_2 tail using a different instrument and calibration method than ours and results for overlapping dates in April 2006 show similar trends.

In a comprehensive overview of the theoretical processes affecting the lunar atmosphere, Smyth and Marconi (1995) point out that the motion of the Earth–Moon system about the Sun has annual variations that affect the lunar sodium tail. These variations are due to the changing radial velocity of the Moon with respect to the Sun: (1) as the Moon orbits the Earth and (2) as the Earth (and Moon) orbit the Sun. As seen from the Sun, the lunar radial velocity is greatest towards the Sun during terrestrial northern latitude Fall at third quarter phase, and is greatest away from the Sun during terrestrial northern latitude Spring at lunar first quarter

Please cite this article in press as: Matta, M., et al. The sodium tail of the Moon. Icarus (2009), doi:10.1016/j.icarus.2009.06.017

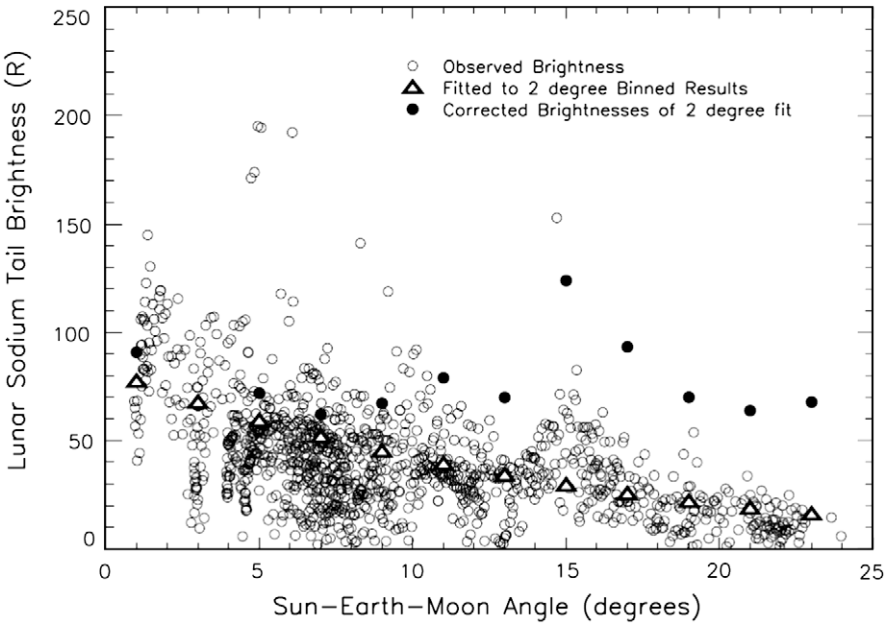

Fig. 4. Results for geometrical corrections to all lunar sodium tail brightness measurements made between April 2006 and October 2008. Hollow circles give the 1239 calibrated brightness values from the 58 nights of photometric class observations. A 2° average was made of the 1239 points which was then used to fit to an exponential function. This fit was used to normalize the data. Triangles are the exponentially decaying function fit to the 2° binned averages. Filled circles show the corrected trend after dividing the 2° averages by the normalized function fit. Sample average (of hollow circles) ~42 R; binned fit average (of triangles) ~38 R; corrected average (of filled circles) ~78 R. Sun–Earth–Moon angles were obtained from the JPL Horizons tool's web interface at http://ssd.jpl.nasa.gov/horizons.cgi. Standard deviations of the 2° average vary between 25% and 60%.

phase. Such variation in radial velocity results in a changing solar radiation pressure seen by lunar sodium atoms that ranges between ~2.60 and 3.15 cm s^{-2}. The consequences suggested are a contracted lunar sodium anti-sunward coma in the Fall and an expanded anti-sunward coma in the Spring when the model assumes stationary sodium atoms with respect to the lunar surface. In this work, we refrain from correcting for day of year variations due to the diverse range of lunar sodium atoms' initial velocities that affect the Smyth and Marconi (1995) suggested model outcomes.

4. Results

The brightness values in Fig. 5 for the lunar sodium tail range from a minimum value of 8 R (in June 2008) to a maximum value of 148 R (in March 2007), giving a mean value of 78 R (½ × (minimum + maximum)). The sample average of all nightly measured brightness values is 71 ± 30 R.

As mentioned earlier, the lunar sodium tail was calibrated to Rayleighs using standard stars. Cases arose where stars were af-

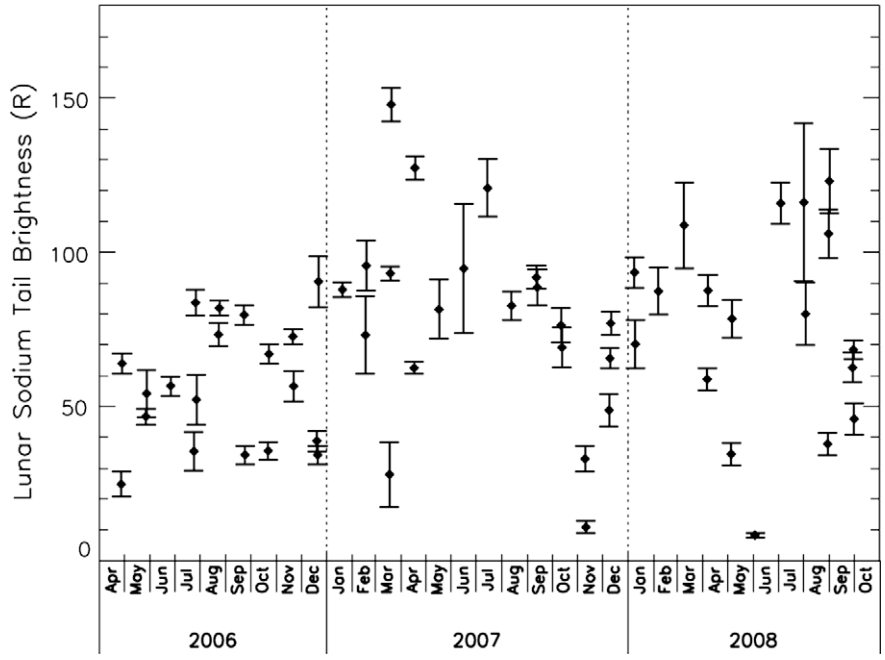

Fig. 5. Brightness values of lunar sodium tail for all observations made in this work. Values have been corrected for Sun–Earth–Moon geometry and range between 8 R and 148 R. Bars represent errors of the mean from each individual night.

Please cite this article in press as: Matta, M., et al. The sodium tail of the Moon. Icarus (2009), doi:10.1016/j.icarus.2009.06.017

fected by clouds. Poisson statistics were used to calculate signal to noise ratios and uncertainties for each night. Data points representing cloudy nights when non-ideal photometric conditions prevailed resulted in fewer images and higher uncertainties (~30%) than during clear nights (~5%).

The 3 × 3 pixel average of the lunar sodium tail feature may be a too narrow sampling of the brightness value for the tail-region in a feature that may reach 9 × 9 pixels at times. Increasing the sample size to 5 × 5 pixels and then to 7 × 7 pixels decreased the average brightness of the lunar sodium tail by ~19% and ~34%, respectively, but otherwise trends in brightness variability remained the same. The median brightness was also determined for the three sample box sizes and resulting values differed from the average by <4%. We maintain that the 3 × 3 pixel average of the lunar tail is sufficient for obtaining a consistent quantitative measure of the core brightness of the lunar sodium spot and is consistent with maximum brightness measurements used by Smith et al. (1999). We re-calibrated the lunar sodium tail discovery images (Smith et al., 1999) using the method described in this paper and, after correcting for geometric effects, found a high but non-exceptional brightness of 126 R.

Another way to present these observations, recalling that the lunar sodium spot was discovered during a meteor shower, is to form an annual pattern of brightness from the 30 months shown in Fig. 5. The monthly average of lunar sodium tail brightness values is shown in Fig. 6. The numbers on the bar of each month represents the numbers of nights of that month that a measurement of the lunar sodium tail was made. The vertical hatches represent the standard deviation of all images available for each month. Brightness values range from a maximum of 94 R in February to a minimum of 43 R in November with an annual average of 71 ± 16 R. The annual variability of lunar sodium tail brightness suggests a quasi-semi-annual trend that peaks in July and February/March with minima in June and November. However, this variability is generally small (about a factor of two) and suggests an overall constancy in the source generating the sodium in the lunar atmosphere.

Taking a more conservative subset of our observations, we experimented with eliminating all photometric nights in which the lunar sodium tail appeared elliptical (i.e. furthest from New Moon time) in the all-sky image and retained only nights with circular-looking lunar tail spots. This eliminated ~27% of nights used, mostly of lower brightness values. The geometric correction fit did not change significantly, and resulted in an enhancement of the March and July monthly-averaged maxima similar to trends shown in Fig. 6. The lunar sodium tail had a maximum brightness of 141 R, a minimum brightness of 32 R and a sample average of 77 R.

5. Discussion

In this section, we look into the three major source processes responsible for generating lunar sodium from the regolith. The dominant source processes are: (1) meteoroid impact vaporization, (2) solar wind sputtering and (3) photon-stimulated desorption. We examine these sources for trends of either constancy or variability when compared with the observed lunar tail brightness values. Since the Leonid meteor shower triggered the discovery of the distant lunar sodium tail (Smith et al., 1999), we begin with discussing the meteor source in some detail first.

5.1. Meteor sources

We are unaware of any published model of annual meteor input for the lunar surface. For the purposes of this work, we estimate a normalized lunar meteoric flux similar to that seen on Earth for both annual shower meteors and annual sporadic meteors.

Shower meteors are taken from the International Meteor Organization (IMO) database between April 2006 and October 2008 that uses visual zenith hourly rates (ZHR). For sporadic meteors, we use individual activity trends of the six known radiants (North Apex, South Apex, North Toroidal, South Toroidal, Helion and Anti-Helion) from Campbell-Brown (2007), as averaged between 2002 and 2005, and since sporadic meteors have nearly annual and slowly varying periods, we make the assumption that the annual trends change little in 2006–2008.

Campbell-Brown (2007) uses the Canadian Meteor Orbit Radar (CMOR) in Tavistock, Ontario (43.2°N, 80.8°W), operating at 29.85 MHz to study meteoric activity. Due to the tilt of the Earth's axis, terrestrial meteor radars at mid and high latitudes in the

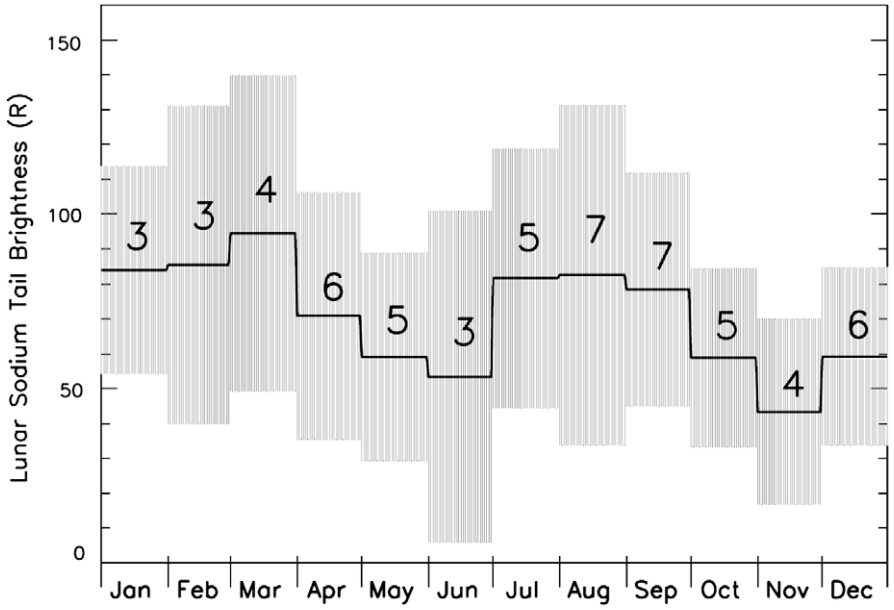

Fig. 6. Monthly average of 58 lunar sodium tail brightness values binned by month from the 30 month observation period. The numbers on the plot are the number of nights with successful brightness measurements for that month over a 2.5 year span. Vertical hatches are standard deviations of brightness values from the average for each month.

Please cite this article in press as: Matta, M., et al. The sodium tail of the Moon. Icarus (2009), doi:10.1016/j.icarus.2009.06.017

northern hemisphere (such as CMOR) can detect ~5 of the 6 sporadic sources (the South Toroidal source lies below their horizon all year and the South Apex is only detectable seasonally). Since South Apex sporadic activity is only available intermittently, we estimate the unavailable rates as being similar in trend to North Apex activity, multiplied by a factor of 1.25, as this is the factor difference between average North Apex activity rates and average available South Apex activity rates. Furthermore, we assume that the South Toroidal source is equal to the North Toroidal one.

The resulting annual trend in meteor activity on the lunar surface is determined by a weighted sum of normalized shower and sporadic meteor activities. Suggs et al. (2008) observed lunar flashes due to ~1 kg size meteoroid impacts between 2006 and 2008 and found that ~44% of impactors were sporadic and ~56% were shower meteors. This is different than percentages detected on Earth by radars due to Earth's atmosphere (see Hawkins, 1956). As a first order estimate, we assume equal weights for each of the seven sources of meteors: the six sporadic sources and the shower source. Next, we consider only the meteors that mostly affect sodium liberation from the lunar surface. Such meteors have been modeled by Bruno et al. (2007) and Cintala (1992) and found to have radii that range between 10^{-8} and 10^{-3} m. Sources that host submillimeter sized meteors are attributed to the sporadic Apex sources (Campbell-Brown, personal communication, 2009). A second model for the lunar meteoric source is then considered from the equal weights of North Apex and South Apex sporadic sources. Both normalized lunar meteoric flux models are shown in Fig. 7 to peak in July and May and to display minimal activity in November, with factors of ~2 difference between maxima and minima.

Both projected annual lunar meteor patterns correlate poorly with observed annual lunar tail brightness in Fig. 6 (~20%) and seem to be insufficient to exclusively account for lunar sodium activity.

Hunten et al. (1991) describe a 60% increase of lunar sodium brightness that was attributed to an unknown lunar meteor shower occurring in October 1990 at ~80° south. This may very well be a sporadic meteor stream from the South Toroidal radiant (~60° S, ~35 km s^{-1}) that has a relative peak in October (Campbell-Brown, 2007). A few years later, the same group noted a less impressive (~17%) but nevertheless increase of lunar sodium brightness due to the 1997 Leonids (Hunten et al., 1998). Verani et al. (1998) also note an increase in lunar brightness that overlaps with the 1995 Leonid meteor shower. Smith et al. (1999) made the discovery of the lunar sodium tail following one of the brightest meteor showers, the 1998 Leonids. Verani et al. (2001) and Barbieri et al. (2001) note that brightness enhancements of the lunar sodium atmosphere occurred during the 1995 and 1997 Leonid but not during the 1999 Quadrantid and 1999 Geminid showers, suggesting that the mean velocity and age (hence abundance of meteoric sodium) of the impacting shower affect the production of sodium gas upon impact with the lunar surface. In summary, evidence linking lunar meteor activity to sodium tail brightness variations has been reported, but in case studies that are intermittent and, in their ensemble, far from conclusive. Using a far larger data set, we are unable to substantiate variability linked to meteors.

5.2. Solar wind source

A solar wind proton striking the lunar surface with a bulk speed of ~400 km/s can cause lunar sodium atoms to be sputtered off the surface and eventually reach the tail. To study the effects of solar wind proton flux onto the lunar surface as a source of sputtered sodium atoms, we use the Charge, Element, and Isotope Analysis System Proton Monitor (CELIAS – PM) instrument on board the Solar and Heliospheric Observatory (SOHO) satellite. SOHO orbits about the first Lagrange point, L1, ~236 R_E (R_E = Earth radius) sunward from the Earth. The satellite's location makes it a good candidate for predicting solar wind effects on the Sun-facing lunar surface during new Moon phase. Similarly, the Solar Wind Electron Proton Alpha Monitor (SWEPAM) instrument on board the Advanced Composition Explorer (ACE) satellite, also orbiting L1, can also be used to study possible solar wind proton effects on the Moon near new phase. Both instruments record bulk speed v and proton density ρ on an hourly basis. A daily average was made of the proton energy density $\sim\rho v^2$ and studied for possible triggers for lunar sodium brightness variability. SOHO and ACE are well correlated (~91%), with the former having a more complete data archive available online, and so only SOHO data is presented here.

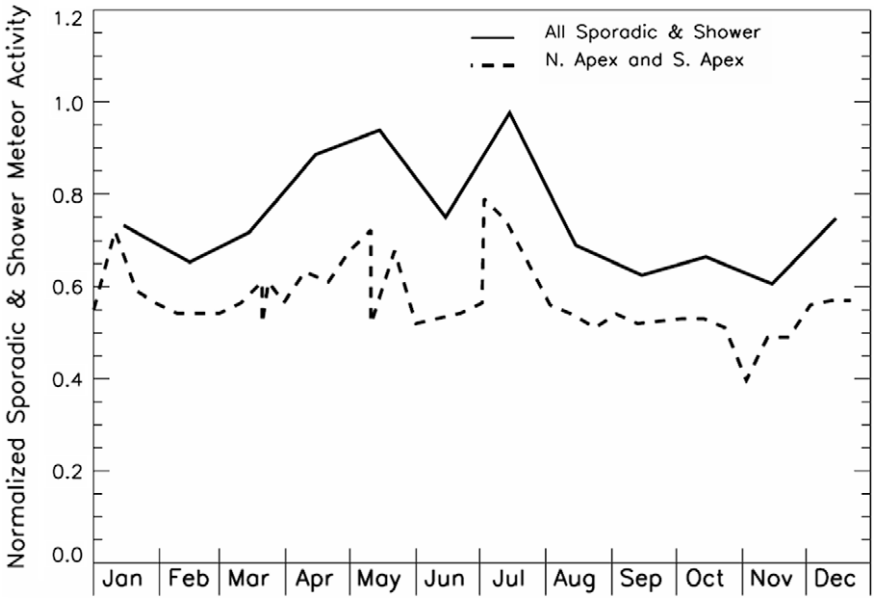

Fig. 7. Composite of sporadic and shower meteor trends projected for the lunar surface averaged annually. Shower meteor activity is taken from the IMO website online database of ZHRs and sporadic meteor activity is taken from Campbell-Brown (2007). The solid line represents all sources with equal weights for each of the six sporadic sources and the shower source. The dotted line represents only equally weighted North and South Apex sources per Campbell-Brown (personal communication).

Please cite this article in press as: Matta, M., et al. The sodium tail of the Moon. Icarus (2009), doi:10.1016/j.icarus.2009.06.017

Our observations of the lunar sodium tail in 2006 show the least variability compared with the other years. The solar wind was more active in 2006 than in 2007 and 2008, when it had a relatively flat profile. A 14–15 December 2006 high activity solar wind period occurred one week prior to the lunar tail observations (20–22 December) and may have just missed the window for possibly impacting the extended tail brightness. We find no evidence in these datasets to link changes in the solar wind to variability in escaping lunar sodium.

The solar wind is mostly composed of protons, electrons and alpha particles. In the analysis here, we consider solar wind protons as a proxy for solar wind energy density, and assume that electrons will not contribute comparably to sputtering off the lunar surface. However, we analyzed alpha particle activity as detected by the ACE SWEPAM instrument and found it to correlate poorly with lunar sodium tail brightness.

5.3. Photon source

For sodium atoms on the Moon, solar photons can be both a source mechanism (via photon-stimulated desorption and radiation pressure that drives sodium atoms aloft back to the lunar surface) and a loss process (via photo-ionization and radiation pressure that drives sodium atoms aloft to escape). Typical energies required to ionize or photo-desorb sodium atoms are ~5 eV (~250 nm) or ~3–4 eV (~400–300 nm), respectively (Yakshinskiy and Madey, 2004). Thus, wavelengths in the near ultraviolet (NUV) range are the most relevant to sodium loss processes on the lunar surface. Here, we look at satellite detected NUV photon fluxes between 200 and 410 nm.

The Solar Radiation and Climate Experiment (SORCE) is an Earth-orbiting satellite that monitors most of the total solar irradiance and detects solar photons with wavelengths between 1 and 2000 nm. Using the Spectral Irradiance Monitor (SIM) and Solar Stellar Irradiance Comparison Experiment (SOLSTICE), we could obtain a solar photon flux integrated between 200 and 410 nm to study effects of solar NUV flux variations on lunar sodium tail brightness. The resulting profile of NUV flux is relatively flat throughout our observation range and decreases slightly in 2008.

For completeness, we also compared lunar sodium tail brightness with X-ray flare sources, F10.7 flux and the geomagnetic Ap index. No strong correlations with tail brightness were evident. The December 2006 disturbance captured in solar wind proton activity also appeared in solar X-ray activity, and the latter also did not cause a lunar tail brightening. The relatively short time period of solar X-ray flares may have an effect on the sodium lunar tail if they occurred ~2 days prior to new Moon. As noted earlier, the December 2006 disturbances occurred on the 14th and 15th, too early to affect the brightness of the lunar sodium tail which was observed on the 20th–22nd. Hence, general photon flux, and specifically NUV flux, does not seem to be the driver of lunar sodium in the tail.

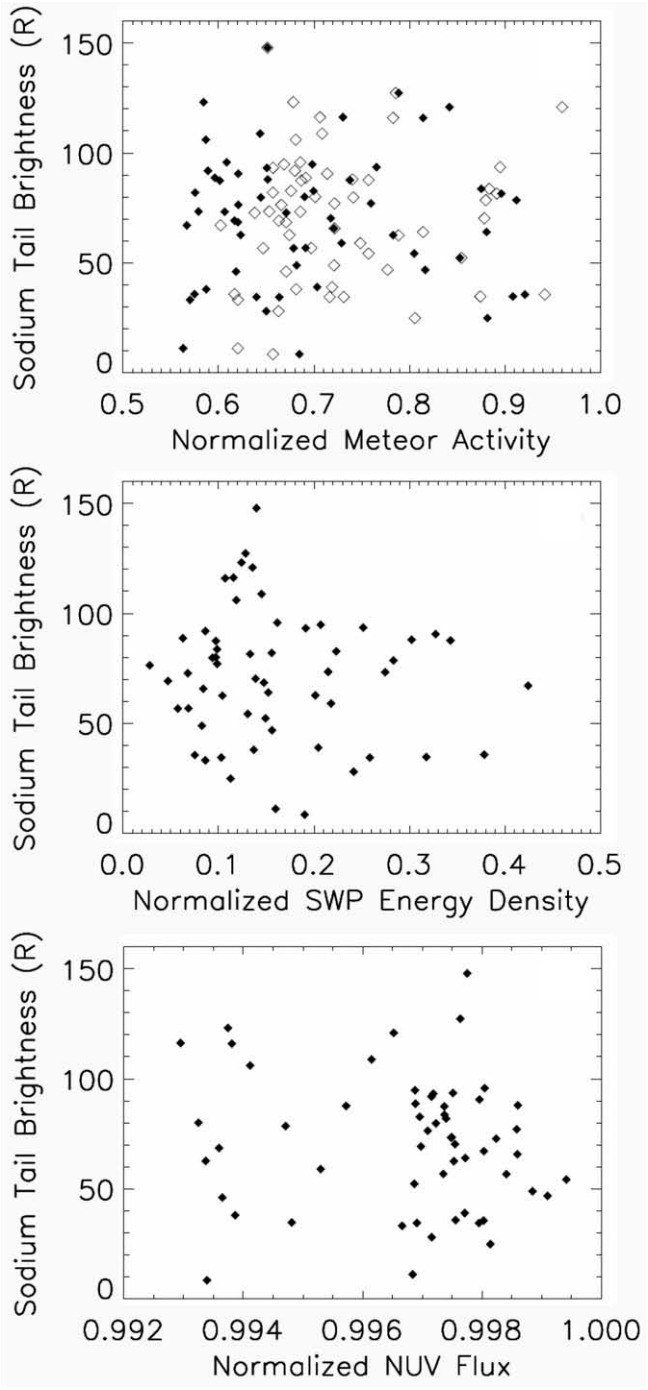

Fig. 8. Scatter plots of lunar sodium tail brightness vs. (a) normalized estimated lunar meteor activity, solid diamonds represent all seven sources, hollow diamonds represent only Apex sources as described in the text, (b) normalized SOHO detected solar wind proton energy density as a proxy for the solar wind sputtering source of sodium on lunar surface, (c) normalized SORCE detected near ultraviolet solar photon flux. In panels (a) through (c), the *x*-axis values are 3 day averages of parameters spanning 4–2 days prior to observation days.

6. Summary

A correlation was done between lunar sodium tail brightness and a 3 day average of the three source activities taken four through 2 days preceding the observation dates (recall that Wilson et al., 1999, estimated a 2 day travel time for lunar sodium atoms to reach our observable region). Fig. 8 represents a summary of this study. In this figure, we plot the lunar sodium tail brightness vs.: the averaged meteor sources in panel (a), the solar wind source in panel (b), and the NUV photon flux source in panel (c). Matching the three source trends with those of lunar tail brightness does not reveal any consistent associations. Lunar sodium tail brightness correlated with meteor activity by ~3% for all sources and ~8% for Apex sources, solar wind activity by ~7%, and photon activity by ~5%. Taking the more conservative subset of our observations, correlations with source processes changed slightly but results remained statistically insignificant.

The short term variability seen in the lunar sodium tail brightness may reflect uncertainties in calibration rather than variability

Please cite this article in press as: Matta, M., et al. The sodium tail of the Moon. Icarus (2009), doi:10.1016/j.icarus.2009.06.017

in the source process, or it may be suggestive of the fundamental base-line variability under solar minimum conditions. We plan to observe the extended tail during a time of higher solar activity to better understand processes that relate source activity to brightness variation. In this study, we conclude that the lunar sodium tail is visible for each lunation, and that no single source is the exclusive driver of sodium off the lunar surface. It is possible that unusual solar minimum conditions and the absence of any appreciable meteor storms play a role in maintaining this ambiguity.

There is room for improvement in future efforts on this topic. The geometric correction done on our data is a rough estimate and would certainly gain validation from a longer set of observations and from incorporating a site-specific viewing angle with the Sun–Earth–Moon angle. Projected lunar meteoric trends are also rough estimates that include only annual meteors and exclude any varying-period meteor streams, and they neglect gravitational corrections for the Earth and Moon. A lunar meteor input function is clearly needed to shed more light on correlations of meteoric impacts to observed brightness variations.

With a renewed interest in the Moon, there is a higher likelihood of sending instruments and life support systems for humans to reside permanently on the lunar surface. Such efforts may cause out-gassing that affect the tenuous atmosphere. We hope to continue these observations to get a better idea of the variability (or lack of it) of lunar sodium tail brightness as a way to improve our understanding of the sources driving this natural mechanism prior to any human induced effects.

Acknowledgments

We would like to thank Dr. Margaret Campbell-Brown for her comments and suggestions, and the timely and helpful reviews of Dr. Gabriele Cremonese, as well as an anonymous reviewer. We would also like to acknowledge the continual cooperation of the director and staff of the Observatory at El Leoncito, Argentina. Publication level data was downloaded from the official websites of the IMO (http://www.imo.net), SOHO (http://sohowww.nascom.nasa.gov) and SORCE (http://lasp.colorado.edu/sorce/index.htm) for daily rates of ZHR, solar wind proton bulk density and velocity, and NUV flux, respectively. We appreciate the data entry efforts of A. Mayyasi, M. Assaf and E. Barris. This work was funded by grants from the Office of Naval Research and the National Science Foundation Aeronomy Program.

References

Barbieri, C., Benn, C.R., Cremonese, G., Verani, S., Zin, A., 2001. Meteor showers on the lunar atmosphere. Earth Moon Planets, 479–486.

Baumgardner, J.L., Flynn, B., Mendillo, M.J., 1993. Monochromatic imaging instrumentation for applications in aeronomy of the Earth and planets. Opt. Eng. 32 (12), 3028–3032.

Bruno, M., Cremonese, G., Marchi, S., 2007. Neutral sodium atoms released from the surfaces of the Moon and Mercury induced by meteoroid impacts. Planet. Space Sci. 55 (11), 1494–1501.

Campbell-Brown, M., 2007. The meteoroid environment: Shower and sporadic meteors. In: Krueger, H., Graps, A. (Eds.), Workshop on Dust in Planetary Systems (ESA SP-643), September 26–30 2005, Kauai, Hawaii, pp. 11–21 (Bibliographic Code: 2007ESASP.643...11C).

Cintala, M.J., 1992. Impact-induced thermal effects in the lunar and mercurian regoliths. J. Geophys. Res. 97, 947–973.

Cremonese, G., Verani, S., 1997. High resolution observations of the sodium emission from the Moon. Adv. Space Res. 19 (10), 1561–1569.

Contarini, G., Barbieri, C., Corrain, G., Cremonese, G., Vio, R., 1996. Spectroscopic observations of the sodium atmosphere of the Moon. Planet. Space Sci. 44 (5), 417–420.

Flynn, B., Mendillo, M., 1993. A picture of the Moon's atmosphere. Science 261 (5118), 184–186.

Hawkins, G.S., 1956. Variation in the occurrence rate of meteors. Astron. J. 61, 386–391.

Hunten, D.M., Sprague, A.L., 1997. Origin and character of the lunar and mercurian atmospheres. Adv. Space Res. 19 (10), 1551–1560.

Hunten, D.M., Kozlowski, R.W.H., Sprague, A.L., 1991. A possible meteor shower on the Moon. Geophys. Res. Lett. 18 (11), 2101–2104.

Hunten, D.M., Cremonese, G., Sprague, A.L., Hill, R.E., Verani, S., Kozlowski, R.W.H., 1998. The leonid meteor shower and the lunar sodium atmosphere. Icarus 136 (2), 298–303.

Mendillo, M., Baumgardner, J., 1995. Constraints on the origin of the Moon's atmosphere from observations during a lunar eclipse. Nature 377, 404–406.

Mendillo, M., Baumgardner, J., Flynn, B., 1991. Imaging observations of the extended sodium atmosphere of the Moon. Geophys. Res. Lett. 18 (11), 2097–2100.

Mendillo, M., Flynn, B., Baumgardner, J., 1993. Imaging experiments to detect an extended sodium atmosphere on the Moon. Adv. Space Res. 13 (10), 313–319.

Mendillo, M., Baumgardner, J., Wilson, J., 1999. Observational test for the solar wind sputtering origin of the Moon's extended sodium atmosphere. Icarus 137 (1), 13–23.

Mierkiewicz, E.J., Line, M., Roesler, F.L., Oliversen, R.J., 2006. Radial velocity observations of the extended lunar sodium tail. Geophys. Res. Lett. 33, L20106.

Potter, A.E., Morgan, T.H., 1988a. Discovery of sodium and potassium vapor in the atmosphere of the Moon. Science 241 (4866), 675–680.

Potter, A.E., Morgan, T.H., 1988b. Extended sodium exosphere of the Moon. Geophys. Res. Lett. 15 (13), 1515–1518.

Potter, A.E., Morgan, T.H., 1991. Observations of the lunar sodium exosphere. Geophys. Res. Lett. 18 (11), 2089–2092.

Potter, A.E., Morgan, T.H., 1994. Variation of lunar sodium emission intensity with phase angle. Geophys. Res. Lett. 21 (21), 2263–2266.

Potter, A.E., Morgan, T.H., 1998. Coronagraphic observations of the lunar sodium exosphere near the lunar surface. J. Geophys. Res. 103 (E4), 8581–8586.

Potter, A.E., Killen, R.M., Morgan, T.H., 2000. Variation of lunar sodium during passage of the Moon through the Earth's magnetotail. J. Geophys. Res. 105 (E6), 15073–15084.

Shiokawa, K., Ejiri, M.K., Ogawa, T., Nakamura, T., 2000. Distant lunar sodium tail observed in the Japanese local-time sector during the Leonid meteor shower of 1998. J. Geophys. Res. 105 (E10), 24621–24626.

Smith, S.M., Wilson, J.K., Baumgardner, J., Mendillo, M., 1999. Discovery of the distant lunar sodium tail and its enhancement following the Leonid meteor shower of 1998. Geophys. Res. Lett. 26, 1649–1652.

Smith, S.M., Mendillo, M., Wilson, J.K., Baumgardner, J., 2001. Monitoring the Moon's transient atmosphere with an all-sky imager. Adv. Space Res. 27, 1181–1187.

Smyth, W.H., Marconi, M.L., 1995. Theoretical overview of the sodium and potassium atmospheres of the Moon. Astrophys. J. 443, 371–392.

Sprague, A.L., Kozlowski, R.W.H., Hunten, D.M., Wells, W.K., Grosse, F.A., 1992. The sodium and potassium atmosphere of the Moon and its interaction with the surface. Icarus 96 (1), 27–42.

Sprague, A.L., Hunten, D.M., Kozlowski, R.W.H., Grosse, F.A., Hill, R.E., Morris, R.L., 1998. Observations of sodium in the lunar atmosphere during international lunar atmosphere week, 1995. Icarus 131 (2), 372–381.

Stern, S.A., 1999. The lunar atmosphere: History, status, current problems, and context. Rev. Geophys. 37 (4), 453–491.

Stern, S.A., Flynn, B.C., 1995. Narrow-field imaging of the lunar sodium exosphere. Astron. J. 109 (2), 835–841.

Suggs, R.M., Cooke, W.J., Suggs, R.J., Swift, W.R., Hollon, N., 2008. The NASA lunar impact monitoring program. Earth Moon Planets 102 (1–4), 293–298.

Tyler, A.L., Kozlowski, R.W.H., Hunten, D.M., 1988. Observations of sodium in the tenuous lunar atmosphere. Geophys. Res. Lett. 15 (10), 1141–1144.

Verani, S., Barbieri, C., Benn, C.R., Cremonese, G., 1998. Possible detection of meteor stream effects on the lunar sodium atmosphere. Planet. Space Sci. 46 (8), 1003–1006.

Verani, S., Barbieri, C., Benn, C.R., Cremonese, G., Mendillo, M., 2001. The 1999 quadrantids and the lunar Na atmosphere. Mon. Not. R. Astron. Soc. 327 (1), 244–248.

Wilson, J.K., Smith, S.M., Baumgardner, J., Mendillo, M., 1999. Modeling an enhancement of the lunar sodium tail during the Leonid meteor shower of 1998. Geophys. Res. Lett. 26 (12), 1645–1648.

Wilson, J.K., Mendillo, M., Spence, H.E., 2006. Magnetospheric influence on the Moon's exosphere. J. Geophys. Res., 111.

Yakshinskiy, B.V., Madey, T.E., 2004. Photon-stimulated desorption of Na from a lunar sample: Temperature-dependent effects. Icarus 168, 53–59.